Water wave scattering by a sinusoidal bed in the presence of vertically sheared current

E. Laffitte, V. Rey, Julien Touboul, K. Belibassakis

Version of Record: https://www.sciencedirect.com/science/article/pii/S0141118721000262
Manuscript_fae6208e32d41cddfca45da895881535

Water wave scattering by sinusoidal bed in the presence of vertically sheared current

E. Laffitte[a,b], V. Rey[a,b], J. Touboul[a,b], K. Belibassakis[c]

[a] *Université de Toulon, CNRS/INSU, IRD, Mediterranean Institute of Oceanography (MIO), UM 110, 83041 Toulon Cedex, FRANCE*
[b] *Aix-Marseille Université, CNRS/INSU, IRD,Mediterranean Institute of Oceanography (MIO), UM 110, 13288 Marseille, FRANCE*
[c] *School of Naval Architecture and Marine Engineering, National Technical University of Athens, Zografos 15773, Athens, GREECE*

Abstract

Wave scattering over a sinusoidal bottom in presence of a vertically sheared current is investigated experimentally and compared to a modified-mild slope model taking into account a linear vertical shear. Waves were generated in a flume without or with an opposing sheared current and propagated over a patch of 10 sinusoidal bars before dissipating on a beach. The shear of the current was controlled using a perforated screen. The Doppler shift of resonant Bragg frequency in the presence of a sheared current is observed experimentally. The modified mild-slope model taking into account both incoming and reflected waves predicts both the location and the amplitude of the peak of reflection at the Bragg resonance conditions, which are found to be sensitive to both the surface current intensity and on the vertical shear.

Keywords: Water waves, scattering, Bragg resonance, Doppler effect, vertically sheared currents

1. Introduction

Wave reflection by periodical topography is widely studied, particularly for its possible role in coastal protection (Bailard et al. (1990), Heathershaw (1982)). Davies (1982) and Davies and Heathershaw (1984) showed theoretically and experimentally that waves can be strongly reflected by a series of periodic bars when their wavelength λ is twice the bar spacing L. This kind of resonance, which is due to the multiple interference of waves scattered by

a periodic structure, is known as Bragg scattering in solid-state physics. In the case of a homogeneous mean flow over the water column, wavenumbers, which depend on the wave direction, are modified and resonance frequency is shifted as shown analytically by Kirby (1988) by extending the theory of Mei (1985) for sinusoidal beds in presence of an ambient current. Vertically sheared current are however observed in the nearshore. They can be due to for instance to tides or waves (see, e. g., Soulsby (1990); Haas and Svendsen (2002)), and enhanced by bathymetry (Rey et al. (2014)). Swan (1990) investigated sheared currents experimentally in a wave-current flume of uniform depth. He found that the oscillatory component of the wave motion is strongly dependant upon the vorticity within the current profile. In presence of such vertically sheared currents, a wave of given frequency f in a fixed frame propagates with a higher celerity in the current direction, and with a lower celerity in the opposite direction. The wavelengths of incoming and reflected waves, respectively λ^- and λ^+, then differ, and the Bragg condition becomes $\frac{\lambda^-\lambda^+}{\lambda^-+\lambda^+} = L$. To date, experiments on wave scattering in the presence of inhomogeneous current are rare and have only concerned wave following current conditions. Wave scattering over a sinusoidal bottom in presence of an ambient following current was investigated experimentally by Magne et al. (2005). Waves were generated in a flume with or without current and propagated over a patch of 5 sinusoidal bars before dissipating on a beach. The current was mesured at three immersion depths, enough to observe that it was not uniform, but not sufficient to fully describe its vertical profile. A Doppler shift of resonant Bragg frequencies and the amplification of the wave reflection due to the current were however experimentally observed as already found analytically by Kirby (1988). Recent comparisons of these experimental results with calculations taking into account a vertically sheared current have shown that the peak location depends on vertical shear (Touboul et al. (2016); Hsiao et al. (2020)).

In this study, we experimentally investigate the effect of a vertically sheared current on Bragg scattering by sinusoidal bed in opposing wave-current conditions. For this purpose, a vertically sheared current of uniform vorticity on the entire water column (i.e a linearly sheared current) is imposed upstream (down-wave) the varying topography by the use of a perforated screen. Detailed measurements are carried out for a fine description of the mean current field with or without waves along the flume. The experiment is carried out in the hydrodynamic flume of the engineering school SeaTech, Toulon, France. After a description of the experimental set-up in

section 2, section 3 presents the mean current field characteristics and the observed reflection coefficients with and without current. Experimental results are compared with analytical results of Kirby (1988) and with calculations from a two-equation mild-slope model able to consider strong reflected wave conditions in the presence of a current with a linearly sheared vertical profile. For a given flow rate, the effect of shear on the computed reflection coefficient is discussed. Conclusions follow in section 4.

2. Experimental techniques

2.1. Experimental set-up

Experiments have been carried out in a $10m$ long, $0.3m$ wide and $0.50m$ high wave-current flume (SeaTech, University of Toulon, France). The current is injected in the channel by a hydraulic pump, of maximum flow rate $Q = 0.027m^3s^{-1}$. At the downstream end of the channel, a piston-type wavemaker generates regular waves in the range $[0.5 - 3.5]Hz$ by horizontal motion. At the upstream end, a slopping beach is used to absorb the wave. Both the wave-maker paddle and the beach are elevated to let the water flow in the channel. After a series of tests, the distance between the wavemaker and the bottom was fixed to $0.10m$ in order to insure the quality of the generated waves on the whole frequency range used in the experiments. For this study, a sinusoidal topography $h(x)$ made of wood and epoxy resin, was installed on the bottom with false horizontal bottoms on both ends in order to insure a constant mean water depth $h = 0.22m$ along the flume. The $x - axis$, originated at the wave-maker location, corresponds to the longitudinal axis of the flume, oriented in the generated wave direction, $z - axis$ is vertical upwards, $z = 0$ corresponds to the still water level (see Fig. 1). The ripples amplitude is $a = 0.035m$, with a wavelength $L = 0.5m$. The patch is $5m$ long including 10 wavelengths. For the experiments, data were recorded for wave frequencies ranging from 0.6 Hz to 1.7 Hz with amplitudes between 0.8 and $1.6cm$ ensuring small wave steepness both without current and with a vertically sheared current.

Regular wave measurements through surface deformation were carried out with resistive synchronous wave gauges. Currents were measured by acoustic Doppler velocimeters (Vectrino, Nortek), including two "side-looking" instruments designed for measurements next to the bed. Their volume sampling is

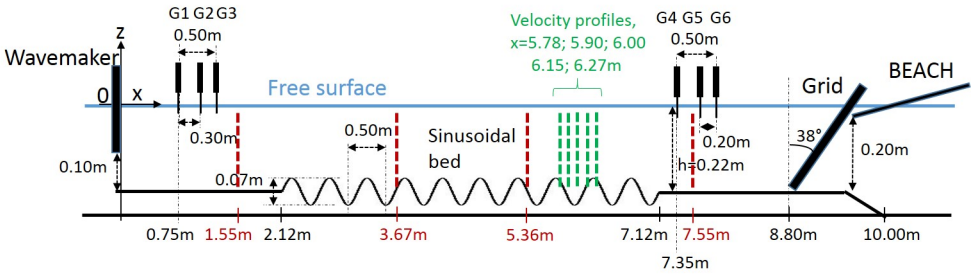

Figure 1: *Experimental set-up. G1 to G6 are the wave gauges, vertical dashed lines correspond to velocity profile measurements with ADV probes*

cylindrical and located at about $5cm$ of the acoustic sensors. In the experiments, the sampling volume was fixed to $9.1mm^3$ with a cylinder's length of $0.24mm$ which allowed a good compromise between the spatial precision of the measurement and the quality of the scattered beams, which was increased by seeding the flow. The frequency sampling was $512Hz$ for the wave gauges and $100Hz$ for the velocimeters. Three probes ahead of the sinusoidal patch (G1-G3) made it possible to separate incident and reflected waves. Series of probes, which could be moved along the flume were displayed every $0.75m$ in order to measure the spatial deformation of the free surface. Currentmeters were used to measure both the near surface mean velocity along the flume and vertical velocity profiles upstream, above and downstream the sinusoidal bed in order to obtain a detailed information on both the evolution of the near-surface current along the flume and on the vertical velocity profile. Both probes and currentmeters locations are given in Fig. 1.

2.2. Sheared current control

In order to control the current profile, the method introduced by Woo and Cermak (1992) and Dunn and Tavoularis (2007) was used. The system consisted in an inclined grid of S-shape at the beginning of the flow and over the entire water column.

The grid was made of 2 mm squares with 1.6 mm holes and was arranged at a mean angle of 35 degrees with the horizontal. From these measurements, a linear fit was applied to get the shear and surface current values. Five synchronous wave gauges recorded the free surfaces at 100 Hz.

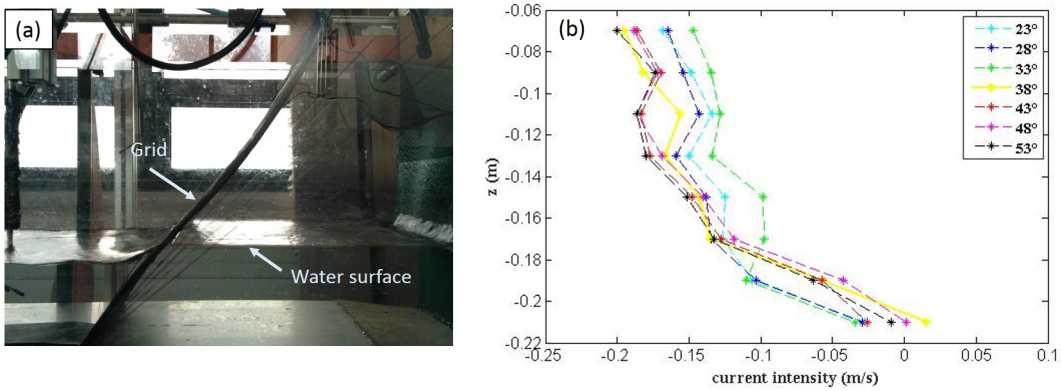

Figure 2: *(a) photograph of the grid; (b) horizontal velocity profiles*

In a previous experimental study in the wave-current flume a curved grid of uniform porosity, $0.29m$ wide and $0.51m$ high was manufactured in order to cover the entire water column with large angles of inclination (Belibassakis et al. (2017)). The porous surface consisted of two grids superimposed with square meshes of inner side $1.5mm$, with a density of 30 meshes per square centimeters. The surface porosity of the grid was $p \approx 0.45$. The pressure drop coefficient K, defined by

$$K = \frac{\triangle p}{0.5\rho U_n^2} \tag{1}$$

where $\triangle p$ is the hydrostatic pressure drop across the grid, ρ the water density and U_n the velocity component normal to the grid, was $K \approx 1.5$.

The choice of uniform porosity was based on the conclusions of Woo and Cermak (1992) which explained that a variation in porosity increases turbulence.

Our grid was made of steel, with a fixed curvature (see Fig. 2a). Our adjustable parameter for the vertical velocity profile was the grid inclination. The angle of inclination θ is measured between the bottom end of the grid and the vertical axis. Velocity profiles in the steady flow were measured by acoustic Doppler velocimeter positioned $1.25m$ downstream of the foot of the grid (see Fig. 1). Their horizontal components are presented in Fig. 2b for θ in the range $[23° - 53°]$ by step of $5°$. Negative values of the current velocity are due to the choice of the x-axis, oriented in the direction of the incident

waves. We can observe that the higher vorticity corresponds to the larger angles. The case $\theta = 38°$ presents the more regular decrease of the horizontal current intensity along the whole water column. It was then chosen for the experiments carried out in the presence of sheared currents (see section 3). During the experiments, the current was first generated, its vertical shape was measured downstream of the grid before the wave generation in order to check the reproducibility of the experiments.

2.3. Wave reflection measurement

The technique used to separate the incident and reflected wave and then calculate the reflection for each wave frequency component is based on least squares method using linear wave theory applied to three probes Rey et al. (2002).

The surface elevation $\eta(x,t)$ for a wave (or wave component) of frequency $f = \omega/2\pi$ is the result of two plane waves, traveling in opposite directions along the x-axis :

$$\eta(x,t) = \left\{ a^- e^{-ik^- x} + a^+ e^{+ik^+ x} \right\} e^{i\omega t} \tag{2}$$

where a^- and a^+ are complex amplitudes. $k^\mp$ are the wavenumbers of the incident and reflected running waves. Assuming a linear vertical shear upwave the sinusoidal bed of the form $U(z) = U_0 + Sz$, they are given by (see for instance Touboul et al. (2016):

$$\left(\omega \pm U_0 k^\pm\right)\left(\omega \pm U_2^\pm k^\pm\right) = \left(\sigma^\pm\right)^2 = g k^\pm \tanh(k^\pm h) \tag{3}$$

with

$$U_2^\pm = U_0 - S\frac{\tanh(k^\pm h)}{k^\pm} \tag{4}$$

In the following, probes are labelled 1, 2 and 3 for simplicity.

The theoretical expression for the free surface at the position of probe G_n based on Airy waves is given for an arbitrary choice of time zero by :

$$\eta_n = \left\{ a_i e^{-i(k^- x_1 + \Delta_n^-)} + a_r e^{+i(k^+ x_1 + \Delta_n^+ + \varphi)} \right\} e^{i\omega t} \tag{5}$$

with $\Delta_n^- = k^-(x_n - x_1)$ and $\Delta_n^+ = k^+(x_n - x_1)$, a_i and a_r are the amplitudes of the incident and reflected wave and φ the phase lag of the reflected wave.

The component of frequency f of the elevation of the free surface as measured by probe G_n $(n = 1, 2, 3)$ is of the form :

$$\eta_n^{(m)} = A_n e^{i(\omega t - \varphi_n)} \tag{6}$$

where superscript (m) indicates the measured values. The amplitude and phase A_n and φ_n are determined from a Fourier analysis of the signal measured by probe G_n. Application of the method of least squares to data from probes G_1 through G_3 leads to the determination of the moduli of the amplitudes of the incident and reflected waves components a_i and a_r

$$|a_i| = \left| \frac{s_2 s_3 - s_{12} s_4}{s_5} \right| \tag{7}$$

$$|a_r| = \left| \frac{s_1 s_4 - s_{12} s_3}{s_5} \right| \tag{8}$$

with

$$s_1 = \sum_{n=1}^{3} e^{-2i\Delta_n^-}; s_2 = \sum_{n=1}^{3} e^{+2i\Delta_n^+}; s_{12} = \sum_{n=1}^{3} e^{+i(\Delta_n^+ - \Delta_n^-)}; \tag{9}$$

$$s_3 = \sum_{n=1}^{3} A_n e^{-i(\Delta_n^- + \varphi_n)}; s_4 = \sum_{n=1}^{3} A_n e^{+i(\Delta_n^+ - \varphi_n)}; s_5 = s_1 s_2 - s_{12}^2 \tag{10}$$

The reflection coefficient R is then given by $R = \frac{|a_r|}{|a_i|}$.

3. Experimental results

3.1. Flow variability along the tank

The flow variability analysis along the tank with or without wave generation is presented in this section before going further into the presentation and the interpretation of the results concerning wave scattering. The mean velocities are calculated by averaging the measured speeds. In the presence of waves, they correspond to the coefficient at zero frequency of the Fast Fourier Transform of the signal. In the experiments, the flow rate is $Q = 0.0106 m^3 s^{-1}$, which corresponds to a mean depth averaged current in the reference frame $U_{mean} = -0.161 m s^{-1}$ for $h = 0.22m$. Bragg resonance

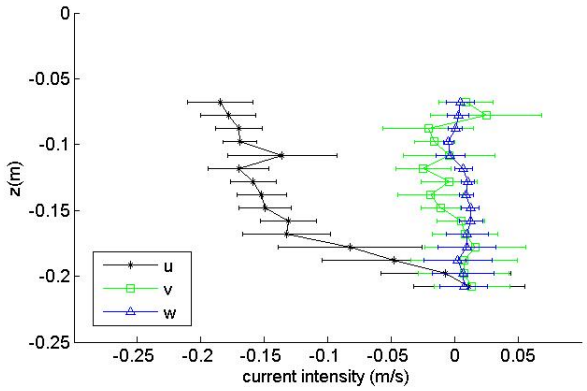

Figure 3: *Measured current intensity upstream, $x = 8.67m$, $(*)$ u, horizontal component; $(\square)$ v, transverse component; $(\triangle)$ w, vertical component.*

is expected when the wave wavelength is approximately twice the bottom spatial period, that corresponds to frequencies in the range $[1.0 - 1.2]Hz$ for the water depth considered, depending on the intensity of the current.

3.1.1. Entrance current characteristics

The three components of the vertical current profile forced by the grid are presented in Fig. 3 for current alone conditions, at location $x = 8.67m$, including standard deviation, indicated by an error bar.

We can observe that the horizontal component of the current is vertically sheared, with a near-surface intensity $U_0 = -0.185ms^{-1}$ for $z = -7cm$ (the negative value is due to the orientation of the frame xOz). We also observe a weaker (respectively higher) shear in the upper (respectively lower) part of the water column, with a standard deviation of about $0.023ms^{-1}$ (respectively $0.048ms^{-1}$). A higher standard deviation is observed for $z = -0.11m$. It is due to the presence of a transverse bar supporting the grid structure. The higher standard deviation near the bottom may be partially due to the current induced vibration at the sensor heads.

After linear regression, such a profile can be characterized by a surface current $U_0 = -0.2085ms^{-1}$ and a vertical shear $S = -0.4283s^{-1}$ in the hypothesis of a constant shear S, as assumed in the numerical calculations presented in section 3.2.3.

The vertical and transverse components are nearly null, with a standard deviation for the transverse velocity component of same order as for the

longitudinal component, and a much lower standard deviation for the vertical component, especially away from the bottom. Velocity intensity fluctuations reveal a turbulent kinetic energy of same order as the mean current kinetic energy.

3.1.2. Mean current evolutions along the flume

Time averaged vertical current profiles were measured at four positions along the flume, downstream (up-wave) the patch ($x = 1.55m$), above (positions $x = 3.67m$ and $x = 5.36m$) and upstream (down-wave)($x = 7.55$), in the absence of waves, and for wave frequencies $f = 0.95Hz, 1.12Hz$, $1.35Hz$ and $1.58Hz$. The choice of these frequencies corresponds both to the range of interest for the Bragg resonance ($[1.0 - 1.2]Hz$) and to a wide range of relative water depth conditions (from almost shallow water to almost deep water conditions).

We can observe in Fig. 4 that the shear intensity diminishes from upstream to above the sinusoidal bed (for decreasing x values), it is then inversed at the end and downstream of the sinusoidal bed, as observed for $x = 3.67m$ and $x = 1.55m$. In contrast to the experiments carried out by Magne et al. (2005) under following wave-current conditions, where the intensity of the surface current remained more or less constant and higher than its intensity in the lower part of the water column over the entire length of the modulated bottom, the opposite is observed in the present experiments, the vertical profile evolving slowly along the modulated bed. The comparison between the vertical profiles of the horizontal velocity components measured for each of the abscissa corresponding to the different wave conditions shows a weak influence of the wave frequency on the vertical profile, especially upstream (down-wave) the sinusoidal bed. A more significant dispersion of the vertical velocity profiles is however observed above and downstream of the patch, demonstrating the effect of the waves on the mean current shape.

The conservation of the flow along the flume implies that the evolution of the vertical shear is linked to that of the surface current U_0. As shown in Fig. 5, the decrease in shear as observed in Fig. 4 leads to a decrease in the intensity of the surface current from $x = 7m$ to $x = 4m$. Its evolution is however more complex in the downstream (upwave) part of the flume, with a greater dispersion of measurements, depending on whether they are the result of experiments carried out in the absence or presence of waves. Whatever the wave conditions, lower velocities are also observed above the troughs, which is consistent with lower depth integrated velocities at larger

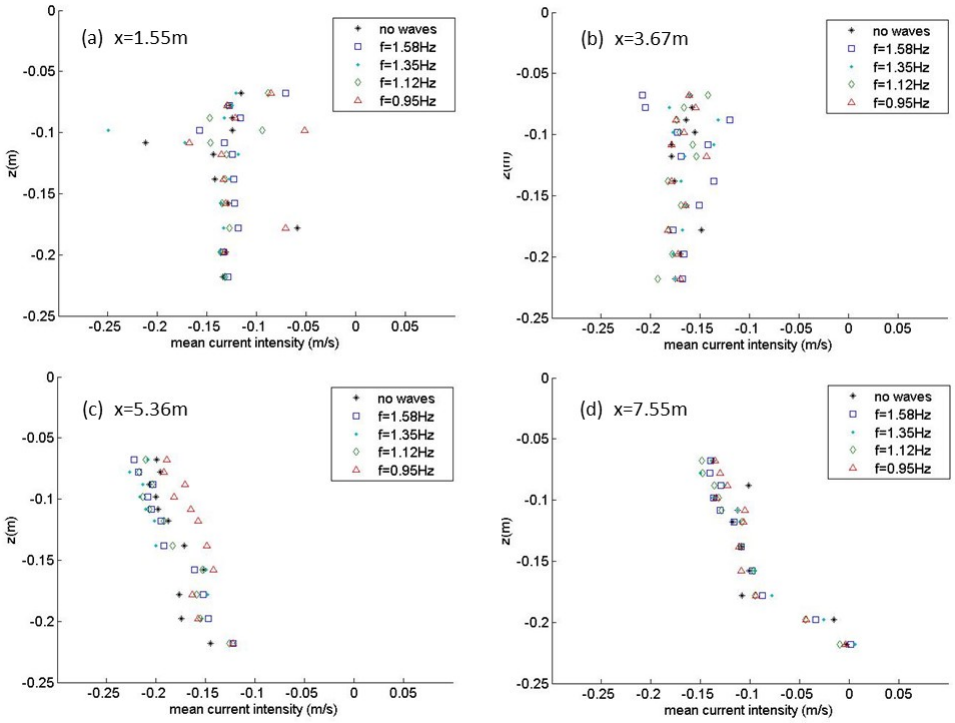

Figure 4: *Time averaged vertical profiles along the flume: (a)* $x = 1.55$*; (b)* $x = 3.67$*; (c)* $x = 5.36$*; (d)* $x = 7.55$*. Hydrodynamic conditions: (*$*$*) current alone, (*$\square$*)* $f = 1.58Hz$*, (*$\bullet$*)* $f = 1.35Hz$*, (*$\diamond$*)* $f = 1.12Hz$*, (*$\triangle$*)* $f = 0.95Hz$*.*

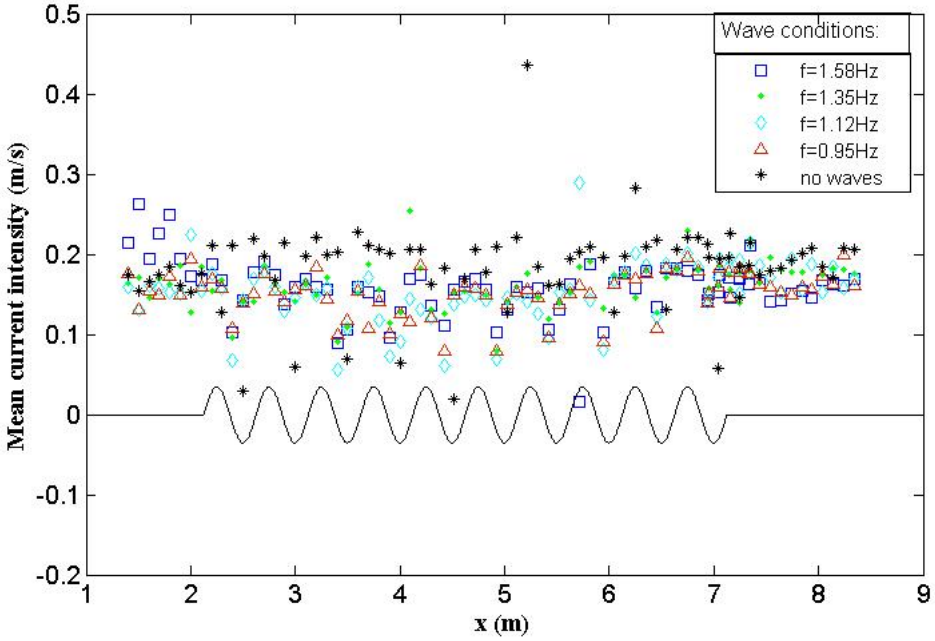

Figure 5: *Time averaged near-surface ($z = -7cm$) horizontal velocity along the flume. Hydrodynamic conditions: ($*$) current alone, ($\square$) $f = 1.58Hz$, ($\bullet$) $f = 1.35Hz$, ($\diamond$) $f = 1.12Hz$, ($\triangle$) $f = 0.95Hz$.*

depths.

3.1.3. Current profile variation at the scale of one bottom wavelength

Due to the depth changes along the sinusoidal bed, one expects the depth averaged mean velocity to be higher above the bottom crests. Time averaged vertical velocity profiles are presented in Fig. 6 at five locations above one bottom wavelength in the absence of waves and for the four above mentioned wave conditions. Whatever the wave conditions, the vertical shear significantly evolves at the scale of one bottom wavelength. In addition, we can observe some influence of the swell on the shape of the vertical profile. It is the most significant at the trough ($x = 6.15$), where the shear observed at the crests and troughs is reversed. In addition, a less sheared profile in the lower part, down to the bottom, is observed for the two lower frequency wave conditions. This may be explained by the stronger wave induced near-bed dynamics for the longest waves. However, no reversed flow is observed along the bottom modulation. Indeed, the bottom is gentle and its wavelength is of order of the wave wavelengths (about half the wavelength at resonance). Unlike the sand ripples formed by the wave induced bottom oscillation, of small extent compared to the wave wavelength, at the origin of vortices, no separation is observed in the present. Nevertheless, there is an evolution of the vorticity at the scale of one bottom wavelength, corresponding to the current profile change, especially near the bed.

3.2. Wave scattering

Wave reflection due to the sinusoidal bed was measured by the use of the three-probes method presented in section 2.3. We first present the experimental results for wave reflection and transmission due to the sinusoidal patch and beach reflection. Reflection coefficient versus frequency with or without current which is then compared to the analytical theory of Kirby (1988), valid for currents presenting an homogeneous vertical structure. Since sheared currents, which were found to slowly vary along the flume, are considered in the present experiments, the sensitivity of both location and amplitude of the maximum of reflection in the Bragg conditions to both surface current and shear are then discussed through comparisons with calculations from a mild slope model adequate for vertically sheared current and strong backscattering.

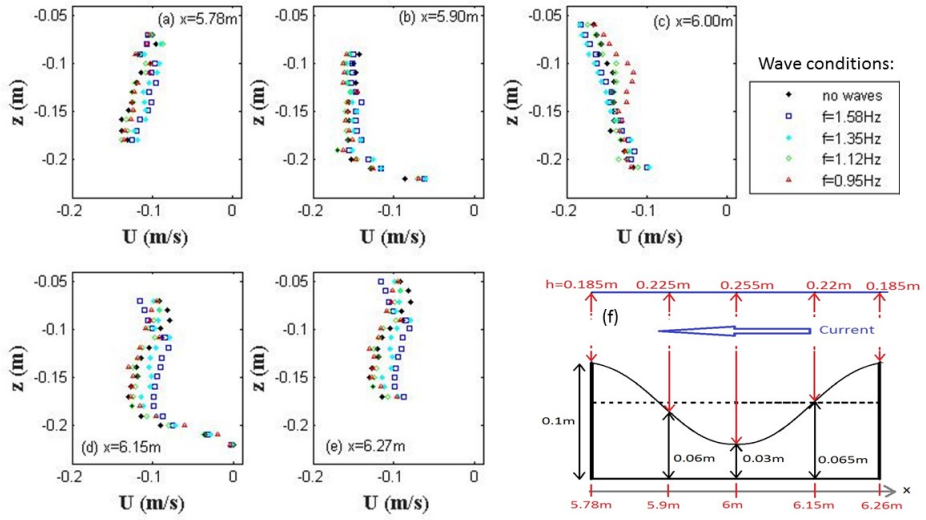

Figure 6: *Time averaged vertical profiles along a bottom wavelength (a)* $x = 5.78$*; (b)* $x = 5.90$*; (c)* $x = 6.00$*; (d)* $x = 6.15$*; (e)* $x = 6.27$*, (f) bottom profile. Hydrodynamic conditions: (*$*$*) current alone, (*$\square$*)* $f = 1.58Hz$*, (*$\bullet$*)* $f = 1.35Hz$*, (*$\diamond$*)* $f = 1.12Hz$*, (*$\triangle$*)* $f = 0.95Hz$

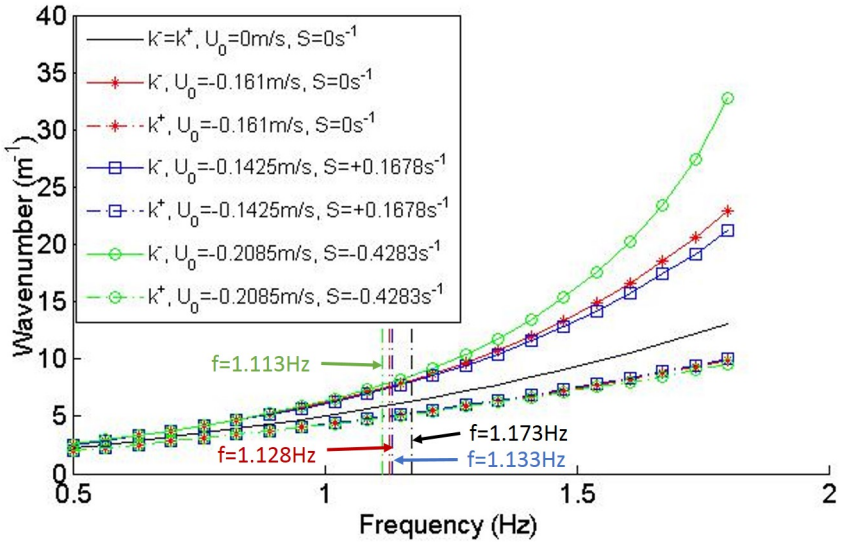

Figure 7: *Computed wavenumber versus frequency; vertical dashlines correspond to the Bragg conditions*

3.2.1. Experimental results on wave scattering

As presented in section 2.3, a three probes technique was used to separate the incident and reflected wave. Wave reflection from the sinusoidal patch is measured from gauges $G1$ to $G3$, at locations $x = 0.75m, 1.05m, 1.25m$, respectively, wave transmission and beach reflection from gauges $G4$ to $G6$ at locations $x = 7.35m, 7.65m, 7.85m$, respectively. At these locations, the water depth $h = 0.22m$ and the vertically averaged mean horizontal current $U_{mean} = -0.161ms^{-1}$. The simplest representation of the vertical current structure assumes a linear evolution of the horizontal velocity component along the $z - axis$. The vertical profile can then be characterized by a surface current U_0 and a constant vertical shear S. Assuming the profile being unchanged between gauges $G1$ to $G3$ (respectively $G4$ to $G6$), $U_0 = -0.1425ms^{-1}$ and $S = +0.1678s^{-1}$ (respectively $U_0 = -0.2085ms^{-1}$ and $S = -0.4283s^{-1}$) after linear regression of the profiles measured at $x = 1.17m$ (respectively $x = 8.67m$) (see fig. 4). In this assumption, wavenumbers are calculated by Eq. 3.

The effect of the current on the wavenumber is presented in Fig. 7, for both uniform vertical current and linearly vertically shear current. Compared

to its value in the absence of current, we can observe that in the presence of current, the wavenumber is smaller for the reflected wave, which propagates towards $x < 0$, as the current flow. It is less sensitive to the shearing than the wavenumber for the incident wave, especially at the highest frequencies. We can also notice that $k^- + k^+ \neq 2k$, k^- and k^+ being the wavenumbers in the presence of current, and k in the case without current. Wave frequency for the Bragg resonance condition, defined by $k^- + k^+ = 2\pi/L$, is indicated by vertical dashed lines in Fig. 7 for the considered current conditions.

Reflection and transmission coefficients of the wave due to the sinusoidal patch and beach reflection are presented in Figs 8.a and 8.b, in the absence and in the presence of current, respectively. In the presence of current, the three probes method is applied by considering either a homogeneous vertical current condition or a linearly vertically sheared current. Beach reflection, defined as the ratio between the reflected wave by the beach and the transmitted wave is also presented.

In the absence of current, we can observe a maximum of reflection of $R = 57\%$ for $f = 1.148Hz$, which is significant and corresponds to $E_R = R^2 = 32\%$ in terms of energy flux. The corresponding wavenumber for both incident and reflected waves is $k = 6.09m^{-1} = 1.94\pi$. The peak then appears at a slightly lower frequency than expected from the Bragg condition $L = 0.5 = \pi/k$, which corresponds to $f = 1.172Hz$. This shift may be due to the finite amplitude of the modulated bed as discussed in Rey (1992) and Guazzelli et al. (1992).

The beach is not fully dissipative since a wave reflection up to 30% is observed at low frequency, that however corresponds to less than 10% in terms of energy. This may be partially due to its positioning near the free surface (see Fig. 1) in order to minimize the perturbation of the current at the flume entrance. On both parts of the resonant peak, the reflection coefficient is under 25%, that corresponds to 6% in terms of energy. In the absence of dissipation, Wave transmission coefficient should be over 97% (94% in terms of energy). We can observe that the transmission coefficient is only of 80% under the peak location, and of order 90% above. This corresponds to a stronger dissipation at low frequency, of order 30%, than at high frequency, of order 13%. Near the peak location, dissipation rate is slightly under 30%. Since shallower water conditions are concerned in the low frequency range, a more significant bottom friction is then observed.

In the presence of current, we can observe a maximum of reflection of $R = 37\%$ for $f = 1.114Hz$. Its amplitude and location are similar when considering either constant or sheared current for the analysis. This is consistent with the small vertical shear observed at the location of gauges $G1$ to $G3$. It is confirmed by the effect of the shear on the Bragg resonant frequency, which shifts from $f = 1.133Hz$ to $f = 1.128Hz$ from $U_0 = -0.161ms^{-1}$ and $S = 0s^{-1}$ to $U_0 = -0.1425ms^{-1}$ and $S = +0.1678s^{-1}$ (see Fig. 7). As for the case without current, the peak then appears at a slightly lower frequency than expected from the Bragg condition, either considering homogeneous or sheared current. It is observed at a lower frequency and it is less significant than in the absence of current, which is partly due to a decrease of the reflected wave amplitude, at given wave energy flux, due to its advection by the current. In fact, the reflecting power of the patch may be seen in terms of wave energy flux. The ratio between the reflected wave energy flux E_R and the incident wave energy flux E_I is given by

$$\frac{E_R}{E_I} = K_D R^2 = \frac{\sigma^+}{\sigma^-}\frac{C^+}{C^-}R^2 \tag{11}$$

where

$$\sigma^{\mp} = \omega \mp k^{\mp}U \tag{12}$$

are the intrinsic radian frequencies in a coordinate system travelling with velocity U ($U < 0$ in this study) and

$$C^{\mp} = \frac{1}{2}\frac{\sigma^{\mp}}{k^{\mp}}\left[1 + \frac{2k^{\mp}h}{\sinh(2k^{\mp}h}\right] \pm U \tag{13}$$

In the present experiments, it then corresponds to $\frac{E_R}{E_I} = K_D R^2 = 21.5\%$, with $K_D = 1.57$, assuming a homogeneous vertical velocity profile, with $U = -0.161ms^{-1}$.

Both transmitted wave amplitude and beach reflection were calculated by considering either constant or sheared current. We can observe in Fig. 8 similar results for the lower frequencies up to $f = 1.25Hz$. For higher frequencies, the strong vertical shear may qualitatively explain the increasing dispersion of the coefficients with increasing frequency. The beach is not fully dissipative. A wave reflection up to 10% is observed at low frequency, that corresponds to less than 2% in terms of energy (K_D varies from 1.3 to 1.9 between $f = 0.7Hz$ and $f = 1.3Hz$). For higher frequencies, beach reflection, which is the ratio between the amplitude of the reflected wave from the beach

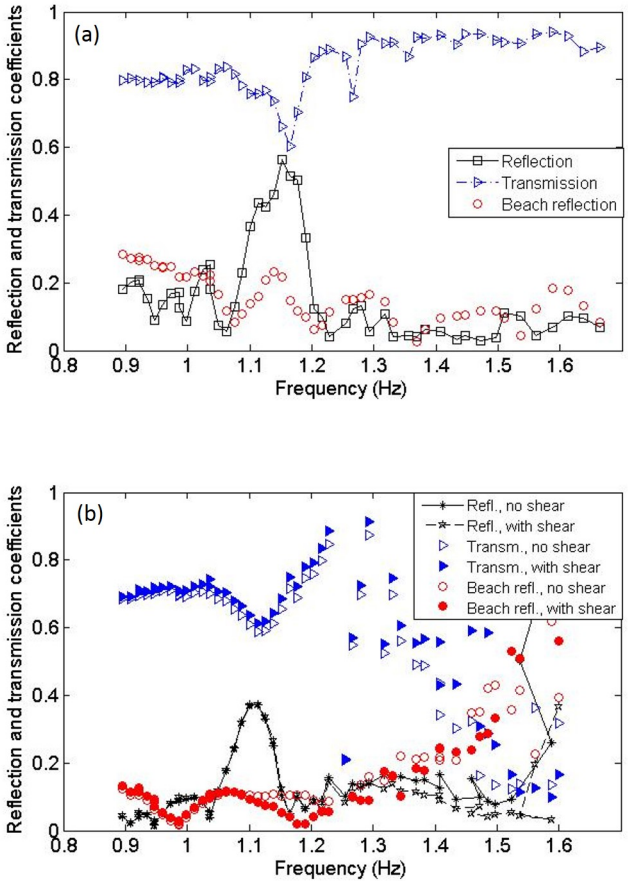

Figure 8: *Wave reflection, transmission and beach reflection versus frequency; (a) without current, (b) in the presence of current*

and the transmitted wave behind the sinusoidal patch, regularly increases up to about 50% for $f = 1.6Hz$. However, its influence on the wave behavior above the patch remains limited since at the same time, the transmission coefficient strongly decreases.

Wave transmission versus frequency follows the same trend as in the absence of current up to frequencies of about $f = 1.3Hz$ but remains smaller. For frequencies under the peak location, wave damping is higher than for frequencies above the peak location, up to $f = 1.25Hz$. For higher frequencies, the three probe method gives less concluding results, opposing current may induce transverse oscillations since wave wavelength is of about twice the channel width for $f = 1.6Hz$.

On both parts of the resonant peak, wave transmission is almost total in the absence of dissipation. In the range $f = 0.9 - 1.05Hz$, the transmitted energy flux is of about 50% in terms of energy. Half of the incoming energy is then dissipated. Near the peak location, dissipation rate is slightly lower, of about 43%. In addition to the bottom friction, wave-current-bottom interactions enhance dissipation.

The reflection coefficient for frequencies in the range $[1.2 - 1.4]Hz$ is of same order (of about 15%) as the beach reflection coefficient. Since at these frequencies the coefficient of transmission remains quite high, this reflection coefficient may be mainly due to the beach reflection.

Experimental results evidence also a strong increase of the reflection coefficient at frequencies above $1.7Hz$, especially with the three probe method assuming homogeneous current. For a homogeneous current of intensity $U = -0.161ms^{-1}$, the incident wave propagates against the current up to a frequency cut-off of about $2.4Hz$. This frequency cut-off decreases down to $1.7Hz$ for $U = -0.23ms^{-1}$. This lower cut-off may contribute to the increasing reflection coefficient found for the frequencies above $1.6Hz$.

Either with or without current, experimental results have shown a significant dissipation, and to a lesser extent, a reflection of the waves by the beach. If one considers the reflected wave to be attenuated after one return path along one bottom wavelength, the interference process will be reduced. It was recently observed for instance for emerging porous media of finite extent (see Arnaud et al. (2017)), that a strong attenuation of the wave reduces the interference process, but does not affect the frequency of occurrence of the maxima and minima of reflection. This means that if the dissipation does not dependent significantly on the frequency around the peak location, we

can expect the location of the frequency peak to be unchanged in the present case, even if its amplitude may be underestimated. Reflection from the beach was found to be weak compared to the incident wave around the resonant peak frequency. In the following, comparisons between the experimental resonant peak amplitude and location and results from either analytical or numerical models are carried out. Due to the low beach reflection near the resonance, its effect is neglected in the calculations and for the discussion of the sensitivity of the peak location with respect to surface current and shear.

3.2.2. Reflection peak sensitivity with respect to vertically averaged current

The measured reflection coefficient with and without sheared current as a function of the wave frequency f is compared with calculations from the theory of Kirby (1988). The analytical method of Kirby (1988) is based on a multi-scale expansion of the potential flow in the presence of a sinusoidal bed of finite extent. As already proposed by Mei (1985) in the absence of current, both the incident and the reflected waves amplitudes are of same order to anticipate the strong reflection at Bragg conditions. The current is assumed homogeneous on the vertical direction. In order to verify the mass flow conservation, this depth averaged current then depends on the water depth. It is modulated above the sinusoidal patch.

In the absence of current, analytical results from Kirby (1988) are in quite good agreement with the experiments, with a peak location at a slighly higher frequency, $f = 1.173Hz$, that corresponds to the above Bragg condition (for this frequency, $k = 6.28m^{-1} = 2.00\pi$) since the model applies for small amplitude ripples.

Analytical results from Kirby (1988) in the presence of current are calculated with the vertically averaged mean current U corresponding to the experimental conditions ($U = -0.161ms^{-1}$) at both sides of the patch. They slightly overestimate both amplitude and location of the peak. As for the case without current, compared to the experiments, peak location is predicted at a slighly higher frequency, $f = 1.128Hz$, which corresponds to the Bragg condition in the presence of current (for this frequency, $k^- = 7.554m^{-1} = 2.404\pi$ and $k^+ = 5.015m^{-1} = 1.596\pi$, hence, $(k^- + k^+)L = 2.00\pi$).

Kirby's results for either $U = -0.129ms^{-1}$ or $U = -0.193ms^{-1}$ are also presented in Fig. 7. We can observe that an error of about 20% for the current intensity results in a noticeable shift of the peak location and a change of its amplitude at a lesser extent. Analytical results for $U = -0.193ms^{-1}$ are in better agreement with the experiments than those using the experimental

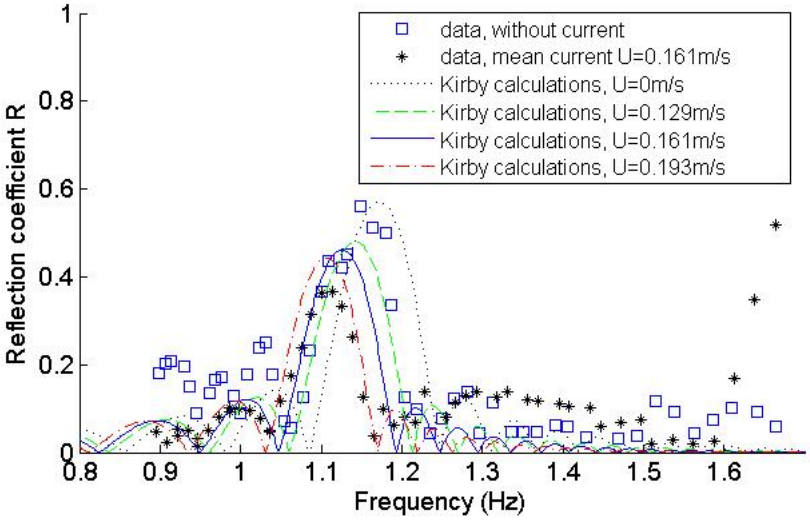

Figure 9: *Wave reflection versus frequency; experiments : (□) without current, (∗) with sheared current, Kirby's results, (−−) $U = 0ms^{-1}$, (−.−) $U = -0.129ms^{-1}$, (. . . .) $U = -0.161ms^{-1}$ (− − . − −) $U = -0.193ms^{-1}$*

depth averaged current $U = -0.161ms^{-1}$. It may be explained by either the shift already observed without current due to the finite amplitude of the bed and/or to a higher near-surface current due to the shear, up to $-0.23ms^{-1}$ above the patch, as shown in Fig. 5.a. In the following, sensitivity of the peak location with respect to the shear is investigated.

3.2.3. Reflection peak sensitivity with respect to surface current and shear

For the purpose of discussing the influence of both the current and its vorticity on the resonant peak, the mild-slope model introduced by Touboul et al. (2016) is adapted. The model initially introduced in this work describes the propagation of water waves in the presence of variable bottom topography, vertically varying, linearly sheared currents, yet showing inhomogeneity in the horizontal directions. For the record, the model was based on a potential description of water waves, which is possible as long as the vorticity is constant. Thus, a variational approach was considered, based on the Lagrangian quantity

$$\mathscr{L} = \int_{-h}^{\varepsilon\eta} -p dz, \tag{14}$$

p referring to the pressure in the fluid, and η to the surface elevation. By reformulating the Bernoulli equation, to take the vorticity into account, this quantity can be expressed analytically. To proceed, though, an assumption is still needed on the form of the elementary solution for the velocity potential, ϕ, which was considered in Touboul et al. (2016) to be

$$\phi(x,z,t) = f(z)\varphi(x,t) = \frac{\cosh(k(z+h))}{\cosh(kh)}\varphi(x,t). \tag{15}$$

A linearization of the Lagrangian quantity, and the application of classical variational calculus led to the formulation of an extended mild-slope equation.

Yet, it was pointed out in Belibassakis et al. (2019) that the hypothesis (15) was too restrictive in configurations involving strong reflection. A comprehensive interpretation can be found in this work. In such cases, another model coupling two mild-slope equations, can be derived. To do so, the hypothesis (15) is relaxed, and replaced with

$$\begin{aligned} \phi(x,z,t) &= \varphi^-(x,t)f_-(z) + \varphi^+(x,t)f_+(z) & (16)\\ &= \varphi^-(x,t)\frac{\cosh(k^-(z+h))}{\cosh(k^-h)} + \varphi^+(x,t)\frac{\cosh(k^+(z+h))}{\cosh(k^+h)}, & (17) \end{aligned}$$

where k^- and k^+ refer to the two solutions of the dispersion equation. Indeed, these solutions, when a current is involved, are not symmetrical anymore, corresponding to a component propagating along the positive x axis, while the second propagates in the opposite direction. These two components are propagating in opposite direction to the current for the first one, and along the current for second one, resulting in a different Doppler shift. As explained in Belibassakis et al. (2019), this can result in a shift of the resonant peak describing the interaction of theses two waves. In the above, $\varphi^-(x,t)$ and $\varphi^+(x,t)$ respectively correspond to the velocity potential associated to the wave propagating along the positive x axis, and the negative x axis.

To acknowledge this asymmetry, the ansatz supported by equation (15) can be introduced in the analytical application of the variational principle. This will result in two coupled mild-slope equations, the system reading

$$\begin{bmatrix} T_{11} & T_{13} \\ T_{14} & T_{12} \end{bmatrix} \begin{bmatrix} \nabla^2\varphi^- \\ \nabla^2\varphi^+ \end{bmatrix} + \begin{bmatrix} T_{21} & T_{23} \\ T_{24} & T_{22} \end{bmatrix} \begin{bmatrix} \nabla\varphi^- \\ \nabla\varphi^+ \end{bmatrix} + \begin{bmatrix} T_{31} & T_{33} \\ T_{33} & T_{32} \end{bmatrix} \begin{bmatrix} \varphi^- \\ \varphi^+ \end{bmatrix} = \begin{bmatrix} 0 \\ 0 \end{bmatrix}. \tag{18}$$

In the above, the coefficients T_{11} to T_{33} are given by

$$\begin{array}{rcl}
T_{11} & = & \langle f_-, f_- \rangle - U_0 U_{2-} \\
T_{12} & = & \langle f_+, f_+ \rangle - U_0 U_{2+} \\
T_{13} & = & \langle f_+, f_- \rangle - U_0 U_{2+} \\
T_{14} & = & \langle f_+, f_- \rangle - U_0 U_{2-} \\
 & & \\
T_{21} & = & \nabla \left(\langle f_-, f_- \rangle \right) - \nabla \left(U_0 U_{2-} \right) + i\omega \left(U_0 + U_{2-} \right) \\
T_{22} & = & \nabla \left(\langle f_+, f_+ \rangle \right) - \nabla \left(U_0 U_{2+} \right) + i\omega \left(U_0 + U_{2+} \right) \\
T_{23} & = & \nabla \left(\langle f_+, f_- \rangle \right) - \nabla \left(U_0 U_{2+} \right) + i\omega \left(U_0 + U_{2+} \right) \\
T_{24} & = & \nabla \left(\langle f_+, f_- \rangle \right) - \nabla \left(U_0 U_{2-} \right) + i\omega \left(U_0 + U_{2-} \right) \\
 & & \\
T_{31} & = & \omega^2 - \left\langle f'_-, f'_- \right\rangle + i\omega \nabla \cdot U_0 \\
T_{32} & = & \omega^2 - \left\langle f'_+, f'_+ \right\rangle + i\omega \nabla \cdot U_0 \\
T_{33} & = & \omega^2 - \left\langle f'_+, f'_- \right\rangle + i\omega \nabla \cdot U_0.
\end{array} \tag{19}$$

Here, the notation $\langle f, g \rangle$ refers to the scalar product $\int_{-h}^{0} f(z) g(z) dz$, and notations U_0, U_{2-} and U_{2+} are respectively the surface current, the current at the depth $2d_c(k^-)$ and the current at the depth $2d_c(k^+)$. Full details of the derivation can be found in Belibassakis et al. (2019).

As shown in section 3.1, the current field more or less depends on the wave conditions. In addition, we also observed that the surface current is modulated above the sinusoidal patch. In order to study the sensibility of the reflection coefficient with respect to both the surface current and the shear, we have considered current fields from experimental data by using a polynomial fit of either the surface current $U_0(x)$ or the shear $S(x)$ along the flume. When $U_0(x)$ (respectively $S(x)$) is extrapolated, $S(x)$ (respectively $S(x)$) is deduced by applied the mass flux conservation.

The discussion on the combined effects of shear and current on scattering was carried out by comparing the results obtained for the different current fields measured as a function of hydrodynamic conditions. The reflection coefficient as a function of the wave frequency f is presented in Fig. 10.a (respectively Fig. 11.a) for surface current (respectively shear) extrapolated from velocity fields measured in the absence of wave, and in the presence of waves, for $f = 1.58Hz$, $f = 1.35Hz$, $f = 1.12Hz$ and $f = 0.95Hz$. Corresponding shear and surface current along the flume are given in Figs 10.b and Figs 10.c (respectively Fig. 11.b and Fig. 11.c).

As a general trend, we can observe in Fig.10.a and Fig.11.a that both peak location and amplitude are correctly recoved by the mild slope method

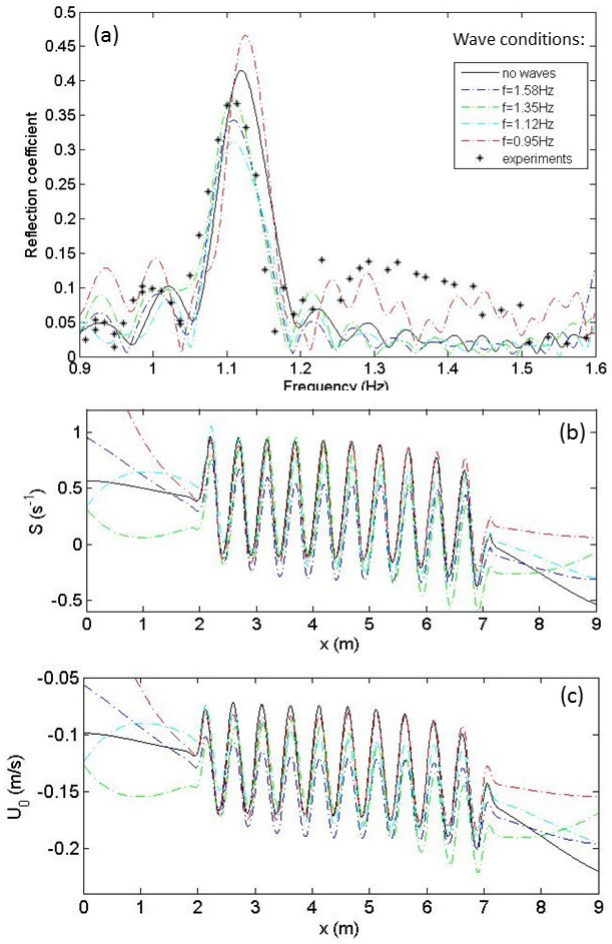

Figure 10: *(a) Wave reflection versus frequency, (b)* $S(x)$*, (c)* $U_0(x)$

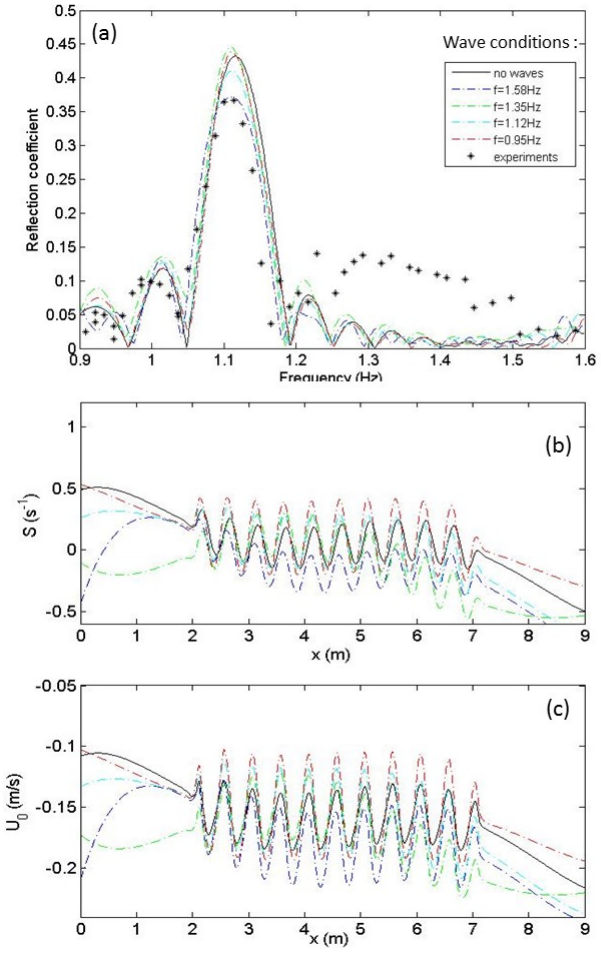

Figure 11: *(a) Wave reflection versus frequency, (b)* $S(x)$*, (c)* $U_0(x)$

whatever the current fields considered, even if, as shown by either Fig.10.b and Fig.10.c or either Fig.11.b and Fig.11.c, significant differences are observed for the current conditions on both sides of the patch, according the the conditions of current field measurements (current alone or at given frequency). The major discrepency is observed with the surface current fitting for $f = 0.95Hz$. It can be explained by the inaccurate values of both U_S and S on downstream (upwave) of the patch.

The common point of the mean current fields considered in Figs. 10 and 11 is a same flow rate along the flume (vertically averaged current which only depends on the local water depth). The overall good agreement observed between experimental data and calculations for the peak location shows that the Bragg resonance conditions are correctly recovered by considering the mean flow rate in the present experiments. It was however demonstrated that the vertical shear had an influence of the peak location and its amplitude from comparisons with the experiments of Magne et al. (2005) ((Touboul et al. (2016); Hsiao et al. (2020)). We observe here at a lesser extent the influence of the vertically sheared current. It can be explained by the slow variation of the shear intensity, which diminishes from upstream to above the patch (for decreasing x values), and is inversed at the end of the patch. As a consequence, the shift observed in the above section for the analytical calculations of Kirby (1988) is not due to the shear but rather to the finite but not small sinusoidal bed amplitude, as already pointed out in the absence of current (Rey (1992); Guazzelli et al. (1992)).

4. Conclusions

Effect of currents on the scattering of surface gravity waves over a sinusoidal bottom was investigated in this study for regular gravity waves. Theories by Kirby (1988), including vertical homogeneous current effects, and by a modified version of the mild slope model of Touboul et al. (2016) for strong backscattered conditions were used for the analysis and the discussion of the experimental results.

In order to generate vertically sheared currents, a grid system was proposed and installed upstream the sinusoidal patch. We have observed a small scale turbulence due to the grid holes, and a pressure drop across the grid. The vertical profile is not conserved along the flume, either for the current alone or in the presence of waves. The regular decrease of the vertical shear, from the grid to the wavemaker, may be due to both the turbulence and

to the presence of the sinusoidal patch. In the presence of wave, both the surface current and the vertical profile are weakly modified, that means that there is a full interaction between the current and the waves. Even if currents characteristic may be affected by the waves, experiments evidenced the Bragg resonance characteristics for waves propagation over sinusoidal bottom in the presence of vertically sheared current. In addition, the spatial modulation of the current along the patch, due to the varying depth, was found to contribute to the reflected energy.

Due to the characteristics of the both analytical and numerical models, which both assume a given established current, comparisons with the experiments and discussions were carried out for given current fields for the whole range of frequencies considered. The shift of the maximum of reflection qualitatively agrees with the effect predicted by Kirby (1988) assuming uniform vertical current. Comparisons with the mild slope model were carried out for extrapolated velocity fields from measurements in the absence or in the presence of waves, assuming either a constant surface current or constant shear above the sinusoidal patch. The effect of the shear on the interference process leading to the Bragg scattering was confirmed. It was found that the interference process was sensible to the current field but remained in quite good agreement with the experiments whatever the extrapolated current field.

Most of the wave propagation models, which restrict to a parabolic form of the propagation equation, assume progressive waves. In the presence of current, the wave wavenumber depends on their respective directions. This must be taken into account in the velocity potential expression as mentioned by Belibassakis et al. (2019). In this condition, the mild slope model proposed by Touboul et al. (2016) for linearly vertical sheared currents is able to correctly predict the location of the peak of reflection for smooth beds. Let us note that in their former version strickly valid for progressive waves, Touboul et al. (2016) have shown that their model correctly predicted the reflected component of the wave, through comparisons with the experimental results of Magne et al. (2005), for a sinusoidal bottom including only 4 spatial periods. In the present experiments, the patch is composed of 10 wavelengths and Bragg resonant conditions result in a stronger reflection and smaller bandwidth around the reflection peak. Due to both the amplitude and the narrowness of the reflection peak, the present experiments may also be of particular interest for the validation of wave models in such a configuration. Let us remark that the models used for the comparisons assume that only the current has an impact on the waves. We have observed that

the wave has also an impact, even if limited, on the current. However, we have shown that good agreement was found between theory and experiment concerning the peak location and amplitude, which was found to be sensitive to the current intensity and its vertical shear.

5. Acknowledgements

Financial support from the University of Toulon for the visit of K. Belibassakis as invited Professor is acknowedged. The support of the French DGA for the visit of J. Touboul in National Technical University of Athens is also deeply acknowedged.

6. Bibliography

Arnaud, G., Rey, V., Touboul, J., Sous, D., Molin, B., Gouaud, F., 2017. Wave propagation through dense vertical cylinder arrays : Interference process and specific surface effects on damping. Applied Ocean Res. 65, 229–237.

Bailard, J. A., Devries, J. W., Kirby, J. T., Guza, R. T., 1990. Bragg reflection breakwater : a new shore protection method? In: Proc. 22th Coastal Eng. Conf. ASCE, New York, USA, pp. 1702–1715.

Belibassakis, K., Simon, B., Touboul, J., Rey, V., 2017. A coupled-mode model for water wave scattering by vertically sheared currents in variable bathymetry regions. Wave Motion 74, 73–92.

Belibassakis, K., Touboul, J., Laffitte, E., Rey, V., 2019. A mild-slope system for bragg scattering of water waves by sinusoidal bathymetry in the presence of vertically sheared currents. J. Mar. Sci. Eng. 7, 9.

Davies, A. G., 1982. The reflection of water-waves energy by undulations on the seabed. Dynamics of Atmos. and Oceans 6, 207–232.

Davies, A. G., Heathershaw, A. D., 1984. Surface-wave propagation over sinusoidally varying topography. J. Fluid Mech. 144, 419–443.

Dunn, W., Tavoularis, S., 2007. The use of curved screens for generating uniform shear at low reynolds numbers. Exp. Fluids 42, 281–290.

Guazzelli, E., Rey, V., Belzons, M., 1992. Higher-order bragg reflection of gravity surface waves by periodic beds. J. Fluid Mech. 245, 301.

Haas, K., Svendsen, I., 2002. Laboratory measurements of the vertical structure of rip currents. J. Geophys. Res. C5, 3047.

Heathershaw, A. D., 1982. Seabed wave resonance and sand bar growth. Nature 296, 207–232.

Hsiao, Y., Tsai, C.-L., Chen, Y.-L., Wu, H.-L., Hsiao, S.-C., 2020. Simulation of wave-current interaction with a sinusoidal bottom using openfoam. Applied Ocean Res. 94, 101998.

Kirby, J. T., 1988. Current effects on resonant reflection of surface water waves by sand bars. J. Fluid Mech. 186, 501–520.

Magne, R., Rey, V., Ardhuin, F., 2005. Measurement of wave scattering by topography in presence of current. Phys. Fluids 17, 126601.

Mei, C. C., 1985. Resonant reflection of surface water waves by periodic sandbars. J. Fluid Mech. 152, 315–335.

Rey, V., 1992. Propagation and local behavior of normally incident gravity waves over varying topography. Eur. J. Mech. B. Fluids 11 (2), 213–232.

Rey, V., Capobianco, R., Dulou, C., 2002. Wave scattering by a submerged plate in presence of a steady uniform current. Coastal Eng. 47, 27–34.

Rey, V., Charland, J., Touboul, J., 2014. Wave-current interaction in the presence of a three-dimensional bathymetry : Deep water wave focusing in opposing current conditions. Phys. Fluids 26, 096601.

Soulsby, R. L., 1990. Tidal Current Boundary Layers. Vol. 9 of Ocean Eng. Sc., John Wiley, New York, USA.

Swan, C., 1990. An experimental study of wave on a strongly sheared current profile. In: Proc. 22th Coastal Eng. Conf. Vol. 1. ASCE, New York, USA, pp. 489–502.

Touboul, J., Charland, J., Rey, V., Belibassakis, K., 2016. Extended mild-slope equation for surface waves interacting with a vertically sheared current. Coastal Eng. 116, 77–88.

Woo, H. G. C., Cermak, J. E., 1992. The production of constant-shear flow. J. Fluid Mech. 234, 279–296.